

NASA TM X-82

DECLASSIFIED-AUTHORITY-MEMO.US:
2313. TAINÉ TO SHAUKLAS
DATED JUNE 15, 1967



Declassified by authority of NASA
Classification Change Notices No. 113
Dated ** 6/22/67

NASA TM X-82

676

TECHNICAL MEMORANDUM

X-82

EXPERIMENTAL INVESTIGATION OF BASE HEATING AND ROCKET
HINGE MOMENTS FOR A SIMULATED MISSILE THROUGH A
MACH NUMBER RANGE OF 0.8 TO 2.0

By Bruce G. Chiccine, Alfred S. Valerino, and Arthur M. Shinn

Lewis Research Center
Cleveland, Ohio

GPO PRICE \$ _____

CFSTI PRICE(S) \$ _____

Hard copy (HC) 3.00

Microfiche (MF) .65

ff 653 July 65

RECEIVED
NASA, DTD
G. MATHE

N67-31731

(ACCESSION NUMBER)

29

(PAGES)

JMX-82

(NASA CR OR TMX OR AD NUMBER)

(THRU)

(CODE)

33

(CATEGORY)

NATIONAL AERONAUTICS AND SPACE ADMINISTRATION

WASHINGTON

October 1959

CONFIDENTIAL

Dated ** 6/28/67 -

NATIONAL AERONAUTICS AND SPACE ADMINISTRATION

TECHNICAL MEMORANDUM X-82

EXPERIMENTAL INVESTIGATION OF BASE HEATING AND ROCKET HINGE

MOMENTS FOR A SIMULATED MISSILE THROUGH A MACH

NUMBER RANGE OF 0.8 TO 2.0*

By Bruce G. Chicchine, Alfred S. Valerino
and Arthur M. Shinn

SUMMARY

Jet-stream interaction effects including base temperatures, pressures, and aerodynamic hinge moments on the rocket motor were investigated with simulated ballistic missile afterbodies in the Lewis 8- by 6-foot wind tunnel.

The basic model was a wing-supported 7.87-inch-diameter body housing a 1000-pound-thrust rocket operated with JP-4 fuel and liquid oxygen.

Three afterbody geometries producing ratios of rocket-nozzle extension to body base diameter of 0.32, 0.59, and 0.78 were investigated over the Mach number range of 0.8 to 2.0. The 0.32 rocket extension was investigated with an open and closed base, while the 0.59 and 0.78 rocket extensions were studied with an open base only. Each afterbody was investigated at angles of attack of 0° and 5° and/or a 4° rocket gimbal angle.

The 0.32 rocket extension open-base geometry indicated temperatures up to 1100° F inside the base cavity and similarly high temperatures throughout the base region investigated. With the base closed the cavity temperatures decreased to approximately 100° F while the temperatures outside of the firewall generally decreased only slightly. Increasing the rocket extension ratio to 0.78 decreased base temperatures approximately to tunnel stagnation values.

No aerodynamic hinge moments were experienced on the rocket engine with the 0.32 rocket extension. Upon increasing the extension ratio to 0.59 and 0.78, however, aerodynamic hinge moments were induced on the

*Title, Unclassified.



exposed rocket engine. Generally, moment forces decreased with decreasing extension ratio, Mach number, and, to a smaller extent, with increasing jet pressure ratio.

INTRODUCTION

The Lewis center is currently engaged in a wind tunnel program studying effects of interaction between rocket jets and external streams on the afterbody aerodynamics and temperatures of ballistic missiles. At present there is a scarcity of both experimental and analytical solutions for such effects for rocket afterbodies, although the basic mechanism of the flow is similar to flow models reported in references 1 to 3. These references have considered pressure effects only and the jet parameters considered were more closely associated with the conventional turbojet or ramjet configurations. With rocket vehicles, the pressure fields and especially the temperature effects are not readily adaptable to analysis. Here the temperatures depend not only on entrainment of hot gases in the base region but also on the possible burning of the combustible components of the entrained gases.

The configurations presently under study are generally distinct from typical turbojets or ramjets in that they are characterized in their physical appearance by cylindrical afterbodies, blunt bases with relatively large base-to-jet area ratios, gimballing nozzles extending beyond the base of the body, and small auxiliary turbine exhaust nozzles. Also, in contradistinction to turbojet or ramjet cases, the characteristics of the base flow field with the present configurations are associated with high ratios of jet to stream total pressure, high exhaust temperatures, fuel-rich propellant and turbine drive mixtures, and possibilities of radiant heat flux from the hot gases.

The cone-ogive-cylinder model in the present report was wing mounted and housed a 1000-pound-thrust rocket engine. Effects on base pressure, base region temperatures, and aerodynamic hinge moments were investigated by varying (1) rocket extension ratio, (2) oxygen-fuel ratio, (3) combustion chamber pressure, (4) rocket gimbal angle, (5) angle of attack; and (6) free-stream Mach number.

SYMBOLS

- c^* characteristic velocity, ft/sec
D diameter
h distance from body surface, in.
M Mach number

O/F oxygen-fuel ratio

P total pressure, lb/sq in. abs

P static pressure, lb/sq in. abs

R model afterbody radius, 3.935 in.

r radial distance, in.

a model angle of attack, deg

β rocket engine gimbal angle, deg

δ boundary-layer thickness

Subscripts :

B model body

b base of body

c rocket engine combustion chamber

e rocket exit plane

J pertaining to the rocket jet

2 local external pressure on rocket nozzle

r base of rocket

w wake region

O free-stream conditions

APPARATUS AND PROCEDURE

Tunnel Mach number	2.0	1.6	1.3	0.8
Tunnel static pressure, lb/sq in. abs	3.24	4.55	6.25	10.63

The length of the cylindrical afterbodies was varied while a constant model length was maintained to the plane of the rocket exit. Three afterbodies were designed so that the rocket exit plane extended 2.5, 4.6, and 6.1 inches beyond the open base of each shroud as shown in figure 2. A fourth afterbody had a closed base or firewall beyond which the rocket engine extended 2.5 inches. In this report each afterbody configuration will be identified by a rocket-extension ratio (0.32, 0.59, and 0.78) defined as the rocket extension length divided by the body base diameter.

Each afterbody was instrumented with Chromel-Alumel thermocouples in the base cavity or engine compartment and in the plane of the base. Temperatures slightly downstream of the base were measured with a radial rake of four thermocouples spaced as shown in figure 3. The 0.59 afterbody also incorporated an axial temperature rake located $3/4$ inch above the rocket cooling jacket. In addition, each afterbody was instrumented with four equally spaced base pressure orifices. The rocket nozzle was instrumented on the top and bottom of a sheet-metal covering with rows of 12 static orifices spaced at $1/2$ -inch intervals.


A boundary-layer survey was made of the flow field over the cylindrical afterbody 16.29 inches upstream of the rocket exit (fig. 4). Pitot pressure ratios are presented for the flow behind the strut mounting and over the unobstructed portion of the body at Mach numbers of 0.8 and 2.0. The boundary-layer profile immediately downstream of the wing strut appears normal (fig. 4); the inflection of the profile in the pitch plane is possibly due to flow disturbances from the model support.

The 1000-pound-thrust rocket engine was water cooled and operated with liquid oxygen and JP-4 fuel. The liquid oxygen was pressurized with helium or gaseous oxygen while the JP-4 fuel was pressurized with nitrogen.

The rocket nozzle was contoured and had a ratio of jet exit to throat area of 8.0. The internal contour is detailed in figure 1. The rocket engine could be gimballed to 4° in the pitch plane about a point located 7.25 inches upstream of the rocket exit plane.

The combustion chamber was instrumented with pressure orifices for monitoring and recording combustion chamber pressure, and the rocket engine was operated over an oxygen-fuel ratio range of approximately 1.6 to 2.8 at combustion-chamber pressures of 400, 500, and 600 pounds per square inch absolute.

The theoretical variation of characteristic velocity, exit static pressure, and combustion-chamber temperature with oxygen-fuel ratio (from ref. 4) is presented in figure 5. A number of experimental characteristic velocity data points from the present study are also shown.




The ignition of the rocket was accomplished automatically with an external spark and propane and gaseous oxygen as pilot propellants. The spark was supplied by an aircraft engine sparkplug located at the end of a retractable ignitor strut (fig. 1) pivoted from the tunnel ceiling. The plug was centered in a cone-shaped funnel, which collected and concentrated the pilot propellants resulting in successful rocket ignition at all Mach numbers.

Once the pilot propellants were burning and the ignitor was retracted, main propellant burning was established in two thrust levels. With full thrust established, transient temperature data were recorded every 1.3 seconds by an automatic-voltage digitizer. When steady-state conditions were ascertained through monitoring of selected thermocouples, temperatures and pressures were automatically recorded on magnetic tape from which terminal data were computed. All temperatures and pressures reported herein are for steady-state conditions.

RESULTS AND DISCUSSION

A simplified flow model of supersonic jet-stream interaction is shown in figure 6 in order to illustrate those elements that influenced the results of this study. (See ref. 1 for a detailed analysis of the interaction between a "cold" jet and the external stream.) The wake of the base is bounded by a mixing zone of relatively cool external-stream air and by the mixing zone of the hot jet. Portions of the stream air and the jet gases are transported into and mixed together in this wake region. A recirculation or reverse flow is induced by the inability of low-energy flow of both mixing regions to penetrate the pressure rise, which results from the impinging of the jet and external stream. The recirculating jet gases contain combustibles resulting both from combustion inefficiencies and fuel-rich operation (for liquid oxygen and JP-4 fuel the oxidant-fuel ratio O/F for maximum specific impulse is 2.25, whereas the stoichiometric ratio is 3.4). The admixture of external air to the jet gases can result in local or widespread zones of combustible mixtures within the wake. Thus, base-region temperatures are a function not only of the transport of hot gases into the base region, but if an ignition source is present, then also upon the possible burning of portions of the entrained gases. Still another possible source is radiation from the jet and wake.

Heat input from convective sources should be reduced by decreasing the length of the boundary of the wake formed by the jet mixing zone. With other flow parameters constant, this decrease can be accomplished by increasing the extension of the rocket from the base. Extending the motor until the free stream impinges upon it should give minimum feedback of jet gases to the wake. At the same time, however, the pressure rise from the deflection of the stream flow by the motor could produce undesirably high external hinge moments about the motor gimbal point when either the missile or the motor is displaced from its neutral attitude.



In addition to the influence of the geometric parameters of the base hardware (such as motor-to-base area ratio and the motor extension and its exit flow angle), the base flow field is dependent upon all of the parameters that describe the flow and composition of the jet and the external stream. These include such things as boundary-layer thicknesses, Mach number, total pressure and temperature, oxygen-fuel ratios, motor gimbal angle, and body angle of attack. The effects of these variables on base-region pressures and temperatures are discussed in the following sections.

Base Region Temperatures

Effect of oxygen-fuel ratio for an open and closed base. - The effect of O/F on cavity, base, and rake temperatures is shown in figure 7 for the 0.32-rocket-extension ratio with both the open- and closed-base configurations at both a gimbal and a body angle of attack of zero degree. Average tunnel total temperature is indicated on figure 7 as a reference at each of the test Mach numbers. The actual base recovery temperatures (rocket-off) were as much as 50° F below the tunnel stagnation values. Considerable scatter of data is evident at the supersonic Mach numbers; however, curves are faired on figure 7 to indicate the maximum temperature levels.

Temperatures measured with the open-base configuration were generally highest inside the cavity and were on the order of 1100° F at the supersonic Mach numbers (1.6 and 2.0) and 700° F at Mach 0.8. These temperatures represent a rise over tunnel stagnation values of about 1000° and 600° F for the supersonic and subsonic Mach numbers, respectively.

The fact that some cavity temperatures were considerably higher than corresponding base or rake values possibly points to more uniform mixing inside the cavity and the promotion of combustion in this sheltered region of the wake flow. This possibility is given some credence also by the fact that closing the base (and hence reducing the opportunity for mixing of the recirculating gases) tended to decrease the temperatures measured on the base and rake at the supersonic Mach numbers (1.6 and 2.0). Cavity temperatures inside the closed base were approximately free-stream values; these values are significant mainly in this study for showing qualitatively the degree of protection afforded vital internal parts of a missile by a base seal. In an actual missile, the cavity temperatures would depend upon the heat-flux balance established by all the surfaces bounding the cavity such as the seal, the motor, and the missile body.

The variation of temperatures with O/F was appreciably different at subsonic and supersonic speeds with the 0.32 rocket extension (fig. 7).



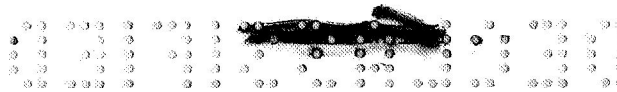
With either the open- or the closed-base configuration at Mach 0.8 there was a slight but uniform decrease in temperatures with increasing O/F . At Mach numbers of 1.6 and 2.0, however, an increase in O/F above approximately 1.8 to 2.0 produced an abrupt temperature increase of as much as $600^{\circ}F$. These higher temperature levels are of more practical interest since they prevail at the optimum oxidant-fuel ratio of 2.25.

There appears to be no obvious explanation for the existence of the two temperature regimes at supersonic speeds, although evidence indicates that combustion or afterburning in the base region is a primary factor. Observations of the flow with motion picture and still cameras did confirm a marked difference in behavior of the stream and jet interaction region between low and high oxidant-fuel ratios. These effects are shown in figure 8. Low temperatures (fig. 8(a)) were generally characterized by a transparent jet and an afterburning region removed downstream from the base a distance of at least 1 body diameter. High temperatures generally were accompanied by a brightly luminescent muff of afterburning, which for these cases began very near the plane of the rocket exit and was quite unsteady. High-speed motion pictures showed wide radial and axial excursions of the flame; frequent flashbacks into the base region of approximately 1/100-second duration could be observed. The unsteady or random nature of the afterburning is emphasized by the wide spread in temperature (fig. 7) measured as steady-state values.

* Effect of rocket extension ratio. - The three open-base rocket extensions were investigated over an oxidant-fuel ratio range of 1.6 to 2.6 at Mach numbers of 0.8, 1.6, and 2.0; temperature data are shown in figure 9. At each Mach number, maximum temperatures decreased markedly in changing from the 0.32 to the 0.59 extension. By comparison with tunnel total temperatures, the 0.78 extension configuration is seen to be essentially free of heat input into the base region. As an example of these temperature reductions, at Mach 2.0 maximum cavity temperatures were 1100° , 230° , and $110^{\circ}F$ for extension ratios of 0.32, 0.59, and 0.78, respectively.

As mentioned previously, increasing the rocket extension decreases that part of the jet boundary from which combustibles and hot gases can be recirculated into the base region. This is shown in figure 9 both by the lowered temperatures for the two longer extensions (0.59 and 0.78) as well as by the independence of these temperatures on variations in O/F . Further indications of the location of the jet and stream intersection are shown in subsequent data.

* Temperature profiles in the base region. - In addition to the radial temperature survey made in the base region of all three afterbodies, an



axial survey was made with the 0.59 rocket extension. These distributions are shown in figure 10 for Mach 2.0 and an oxidant-fuel ratio of approximately 2.2. The radial profile for the shortest rocket extension (0.32) shows higher temperatures at the center, which tends to substantiate the base recirculation pattern presented in figure 6. As the rocket extension was increased and the general temperature levels fell, the radial profiles became flatter; for the 0.7% afterbody the temperatures were essentially uniform across the base. The axial temperature profile for the 0.59 afterbody (fig. 10(b)) indicates an over-all decrease in temperatures with distance from the nozzle exit.

Base Region Static Pressures

Effect of jet pressure ratio on base pressure. - Base pressure ratio is presented in figure 11 as a function of the ratio of computed jet-exit static pressure (from fig. 5(b)) to free-stream static pressure for the three rocket extension ratios studied. Curves are drawn only as a guide to the general trend of the data at a constant free-stream Mach number or constant combustion-chamber pressure inasmuch as base pressures were to some degree affected by oxidant-fuel ratio.

For rocket-on conditions, base pressure ratios decreased from about 0.94 at Mach 0.8 to values as low as 0.54 at Mach 2.0. Base pressures generally decreased slightly with increasing rocket extension and increased from rocket-off to rocket-on conditions; this latter effect was least pronounced for the shortest rocket extension. For all rocket extensions, base pressure appeared to increase with jet pressure ratio at about the same rate. This dependence of base pressure on jet pressure existed even with the 0.78 rocket extension, which was previously shown to be long enough to effectively eliminate heat input to the base from the jet.

Effect of rocket extension on rocket external pressure distributions. - External static-pressure distributions on the rocket nozzle are presented in figure 12 for the three rocket extension ratios (for $\alpha = 0^\circ$, $\beta = 0^\circ$) at Mach 0.8, 1.3, and 2.0. Pressure distributions for both rocket-on and rocket-off conditions are shown in figure 12.

The pressures along the 0.32 nozzle extension were constant and agreed with the base pressure. Both the 0.59 and 0.78 extensions experienced pressure rises on the nozzle ranging from base pressure level to free-stream static pressure. With the rocket off, the axial location of the initial rise in pressure moved upstream in direct proportion to the cutting back of the afterbody shroud. With the rocket on, the same relation was approximately true.

Theoretical inviscid stream and jet boundaries of the base region flow are shown in figure 13 for the three afterbodies at Mach 2.0 and are based on the measured pressures indicated. The streamline from the shoulder of the base was obtained from reference 5, while the initial angle of the jet expansion was computed from the base pressure at the end of the nozzle using reference 6. From figure 13 the relative effects of rocket extension on base temperatures can be deduced from the location of the stream-jet intersection point or from the jet boundary length. Relative air loads on the motor are implied by the proximity of the limiting external streamline to the motor. The inviscid theory, however, predicts no pressure rise on the motors at Mach 2.0 for any rocket-on condition (fig. 13) whereas, as shown in figure 12(a), only the 0.32-extension afterbody was free of such an effect. The actual start of the wake pressure rise for the 0.59- and 0.78-extension afterbodies was on the order of $1/3$ body diameter upstream of that which would be predicted from figure 13(a). (For the 0.78 afterbody it appears that the entire wake pressure rise was completed ahead of the motor exit station.) This disparity between the pressure data and the inviscid streamline patterns indicates the strong influence of actual viscous mixing effects in the base flow field.

Effect of combustion-chamber pressure on rocket external pressure distributions. - External nozzle static-pressure distributions are presented in figure 14 for combustion-chamber pressures of 400, 500, and 600 pounds per square inch absolute for the 0.59 and 0.78 rocket extensions at Mach 2.0. As mentioned previously (fig. 12), motor pressures are uniform at the base pressure value until the start of the pressure rise, the location of which in all cases was independent of chamber pressure. For each configuration the pressures rose to about the same levels. Thus, the higher chamber pressures with their higher base pressures resulted in a slightly decreased over-all pressure rise. Nozzle pressure distributions with the 0.32 extension are not shown in figure 14 since they were relatively flat and varied with base pressure for changes in combustion-chamber pressure.

Aerodynamic Hinge Moments

In computing moments due to the external air loads about the rocket gimbal point, a normal force per unit axial length was determined at each orifice station by arbitrarily assuming a linear circumferential pressure distribution between top and bottom orifices. The hinge moments presented herein are then the numerical integration of the incremental moments attributed to the normal force at each station. In this study, missile angle of attack was achieved by pitching the model nose down; motor gimbal angle was obtained by pitching the nozzle upward. Thus, the engine was gimballed in the direction to restore the missile to zero angle of attack. A positive hinge moment is defined as that which tends to pitch the missile nose up.



The pressure distributions on the top (windward) and bottom (lee-ward) side of the rocket nozzle for 4° gimbal angle or 5° angle of attack and combinations of the two are presented in figure 15. For reference purposes pressure distributions for no-moment conditions ($\alpha = 0^\circ$, $\beta = 0^\circ$) are also included.

Although pressure distributions were not investigated at comparable combinations of gimbal and angle of attack for all configurations, it does appear from figures 14 and 15(a) that increasing the rocket extension ratio increased the level and asymmetry of the pressures acting on the greater exposed areas on the nozzle thus increasing the aerodynamic hinge moment about the rocket gimbal point.

The aerodynamic hinge moments acting on the 0.78 extension computed from these asymmetrical nozzle pressures are presented in figure 16. The moments are presented in terms of model scale and missile full-scale values for a 4° rocket gimbal at angles of attack of 0° (fig. 16(a)) and 5° (fig. 16(b)).

In general, figure 16 indicates an increase in aerodynamic hinge moment with an increase in Mach number for a constant chamber pressure. For example, at zero angle of attack and a 4° rocket gimbal angle (fig. 16(a)), hinge moments increased with Mach number from 900 to 6300 foot-pounds full scale for a combustion-chamber pressure of 500 pounds per square inch absolute. However, for the combination of gimbal angle and angle of attack (fig. 16(b)) increasing the Mach number from 1.6 to 2.0 showed a reversal in direction of the aerodynamic hinge moment about the gimbal point.

The effect of angle of attack in this reversal of moment direction can be deduced from the rocket nozzle pressure distribution for the 0.59 extension in figure 15. (Data were not available for $\beta = 0^\circ$ and $\alpha = 5^\circ$ attitude with the 0.78 rocket extension.) Here both rocket-on and rocket-off data indicate relatively large negative moments. Assuming that similar negative moments exist for the 0.78 afterbody at $\beta = 0$ and $\alpha = 5^\circ$, it is conceivable that these negative values override the positive moments indicated for the gimbal-angle data alone (fig. 16) when gimbal angle is combined with angle of attack.

It is significant to note from figure 16 (by comparing rocket-on and rocket-off data) that valid aerodynamic hinge moments cannot be obtained from models that do not have jet flow; rocket-off data may show erroneous magnitude as well as incorrect direction of the moments.

SUMMARY OF RESULTS

Jet-stream interaction studies using a wing-supported body 7.87 inches in diameter and a 1000-pound-thrust rocket with liquid oxygen and JP-4 propellants at Mach numbers from 0.8 to 2.0 indicated the following:

1. Temperatures in the base region decreased with increasing extension of the rocket beyond the base. For open-base configurations with rocket extensions of 0.32, 0.59, and 0.78 body diameters, **maximum** engine cavity temperatures were 1100° , 230° , and 110° F, respectively, at Mach 2.0. (Tunnel stagnation temperature was 140° F at Mach 2.0.)

2. Base region temperatures were sensitive to oxygen-fuel ratio only with the 0.32 rocket extension and especially so at the supersonic speeds where there was an abrupt increase of as much as 600° F from a low- to a high-temperature regime as the oxidant-fuel ratio increased to values above approximately 1.8 to 2.0.

3. The motor having the shortest extension had external pressures all identical with base pressure and, hence, experienced no externally induced moments about its gimbal point. The pressure rise on the motors having the longer extensions led to moments whose magnitude and direction appear to vary in a nonuniform manner with Mach number for some combinations of gimbal angle and angle of attack.

4. In general, base pressures decreased slightly with increasing rocket extension for rocket-on conditions. For all rocket extensions, base pressure appeared to increase with jet pressure ratio at about the same rate.

5. The external pressure rise on the rocket **motors** occurred considerably farther forward than would be predicted by inviscid theory based on measured base pressures.

Lewis Research Center

National Aeronautics and Space Administration
Cleveland, Ohio, May 8, 1959

REFERENCES

1. Baughman, L. Eugene, and Kochendorfer, Fred D.: Jet Effects on Base Pressures of Conical Afterbodies at Mach 1.91 and 3.12. NACA RM E57E06, 1957.
2. Fuller, L., and Reid, J.: Experiments on Two-Dimensional Base Flow at Mach = 2.4. R. & M. 3064, British RAE, 1958.
3. Chow, Wen-Lung: On the Base Pressure Resulting from the Interaction of a Supersonic External Stream with a Sonic or Subsonic Jet. Paper No. 59-4, Inst. Aero. Sci., 1959.
4. Huff, Vearl N., and Fortini, Anthony: Theoretical Performance of JP-4 Fuel and Liquid Oxygen as a Rocket Propellant. I - Frozen Composition. NACA RM E56A27, 1956.



5. Sims, Joseph L.: Results of the Computations of Supersonic Flow Fields Aft of Circular Cylindrical Bodies of Revolution by the Method of Characteristics. Rep. DA-R-49, Army Ballistic Missile Agency, Mar. 17, 1958.
6. Love, Eugene S., and Grigsby, Carl E.: Some Studies of Axisymmetric Free Jets Exhausting from Sonic and Supersonic Nozzles into Still Air and into Supersonic Streams. NACARM L54L31, 1955.



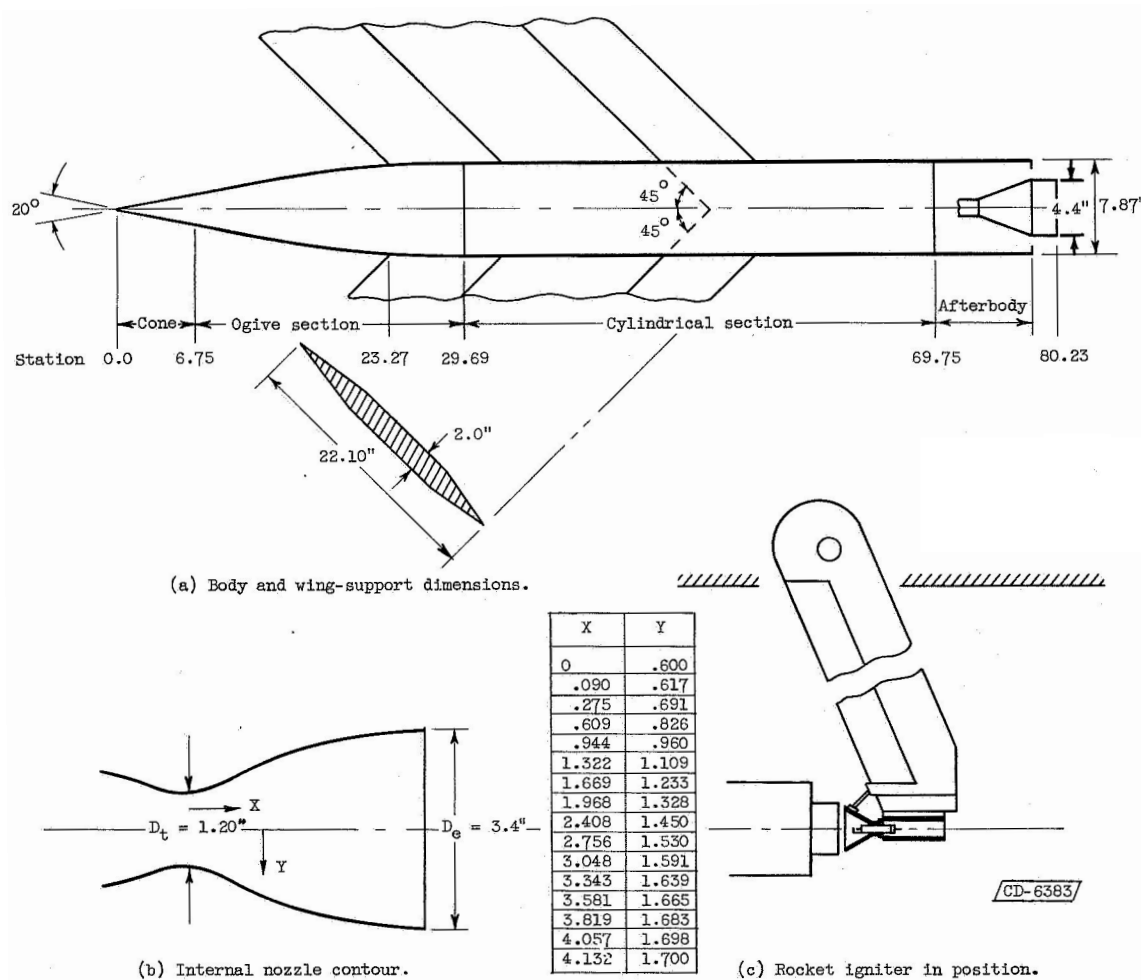
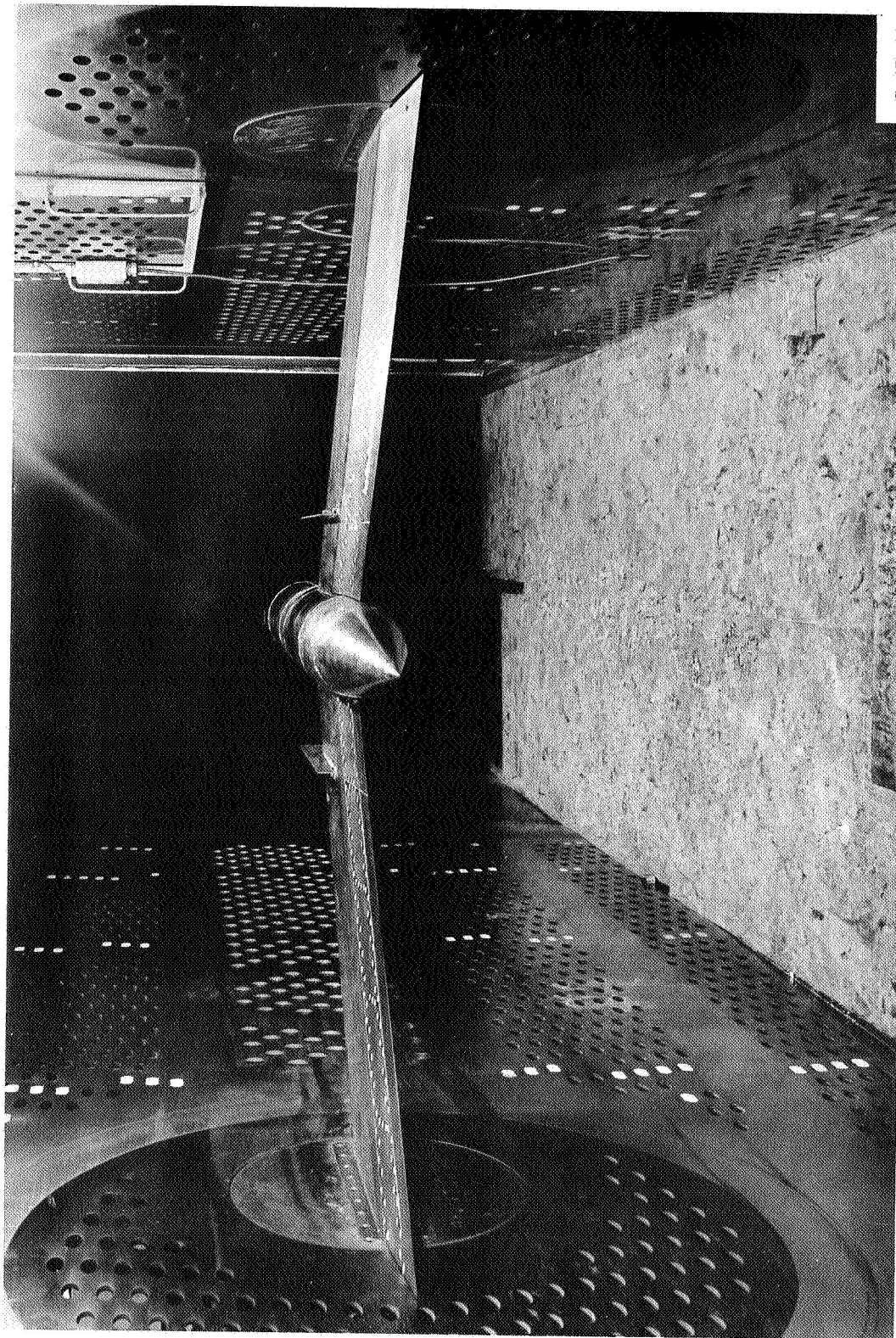
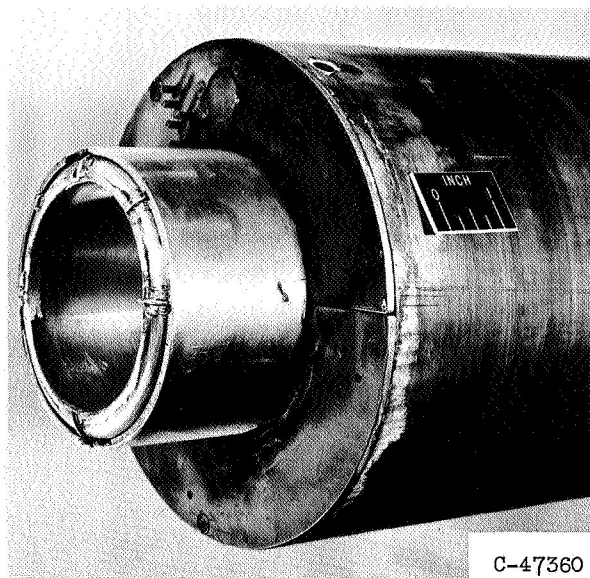


Figure 1. - Schematic drawing of rocket-exit study model.

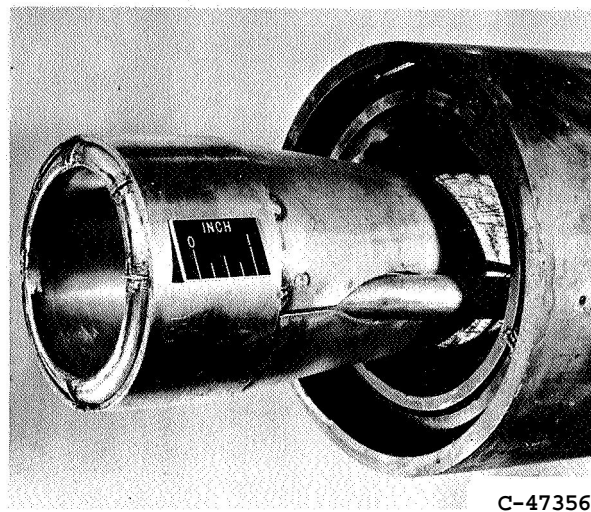


(a) Model mounted in the tunnel test section.

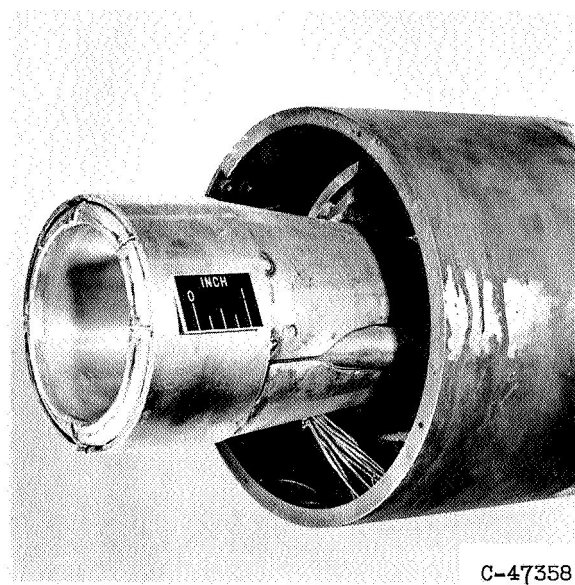
Figure 2 - Model photo graphs.



0.32 Rocket extension (closed base)



0.78 Rocket extension (open base)



0.59 Rocket extension (open base)

(b) Afterbody configurations investigated.

Figure 2 - Concluded. Model photographs.

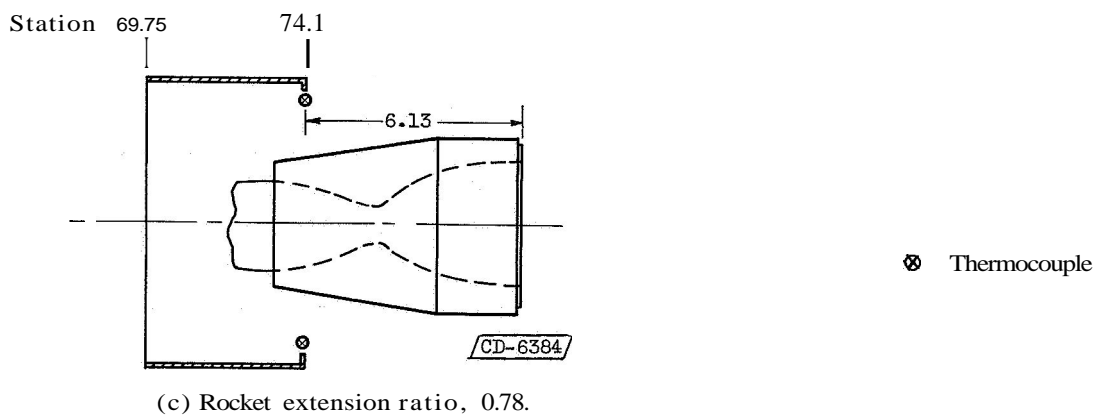
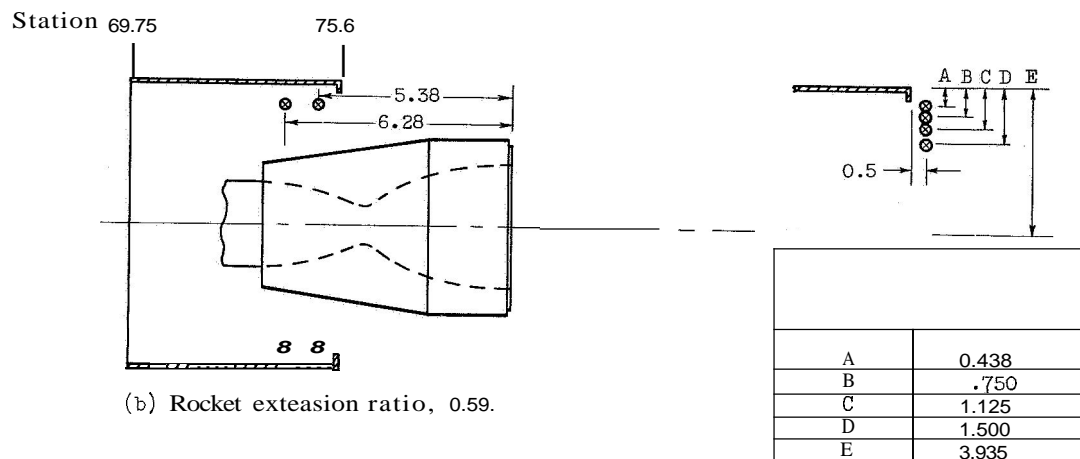
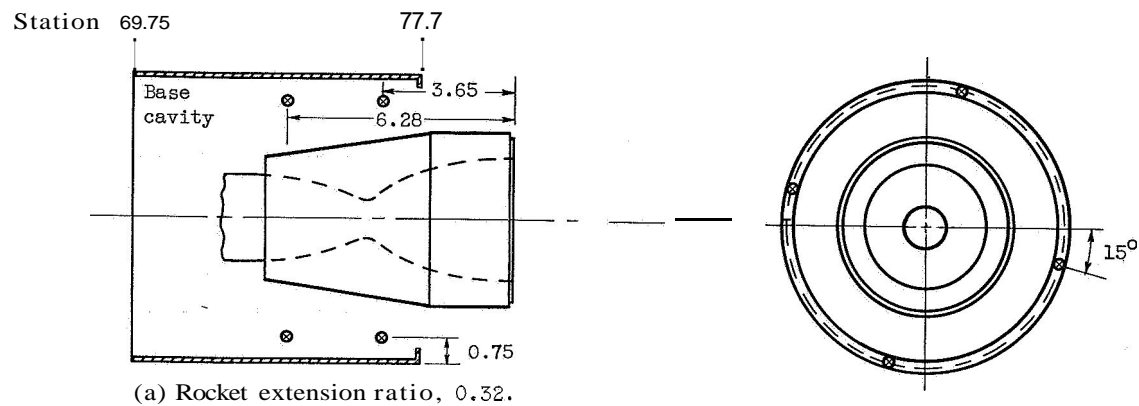


Figure 3. - Rocket-exit study afterbody design and thermocouple instrumentation.
(Dimensions in inches.)

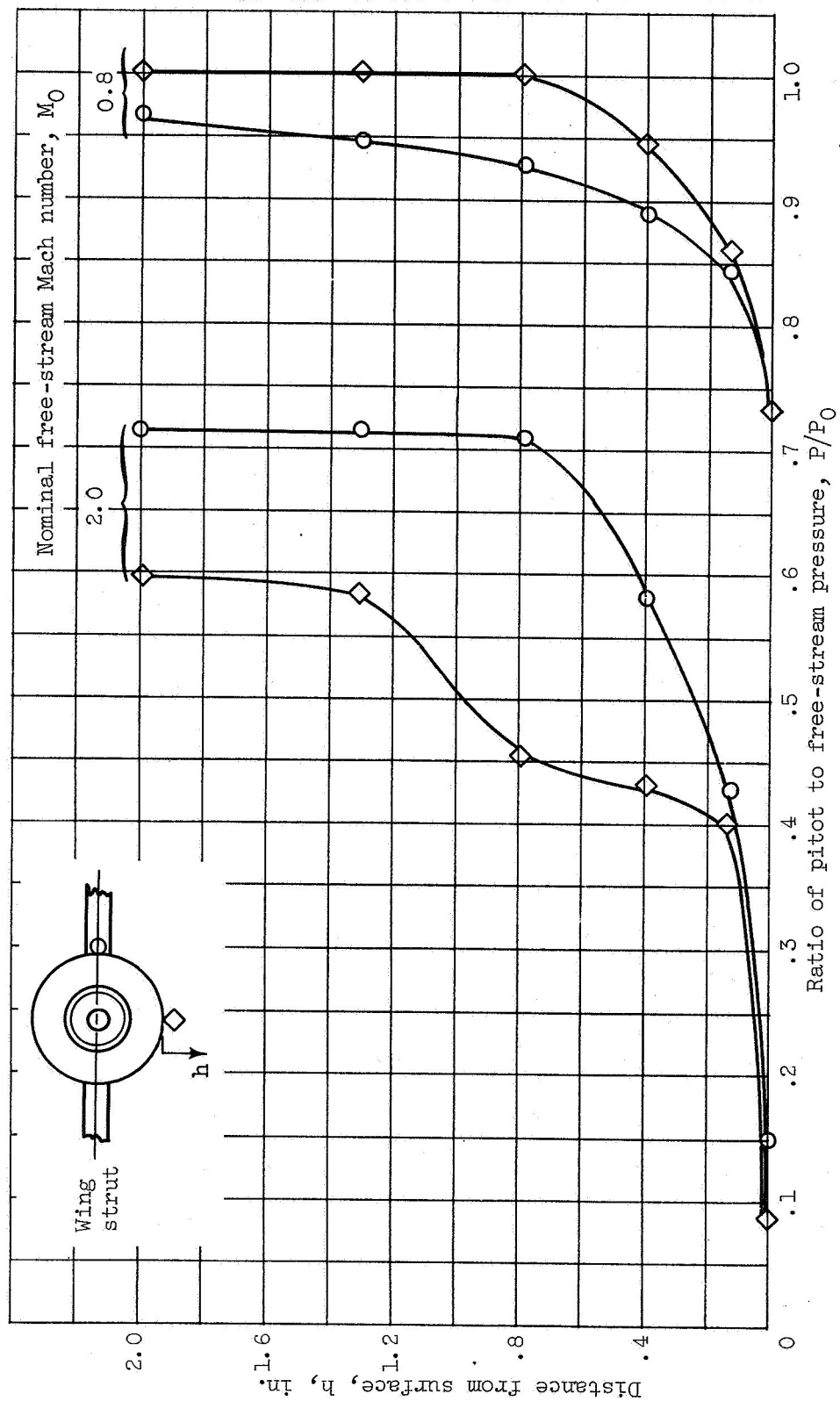
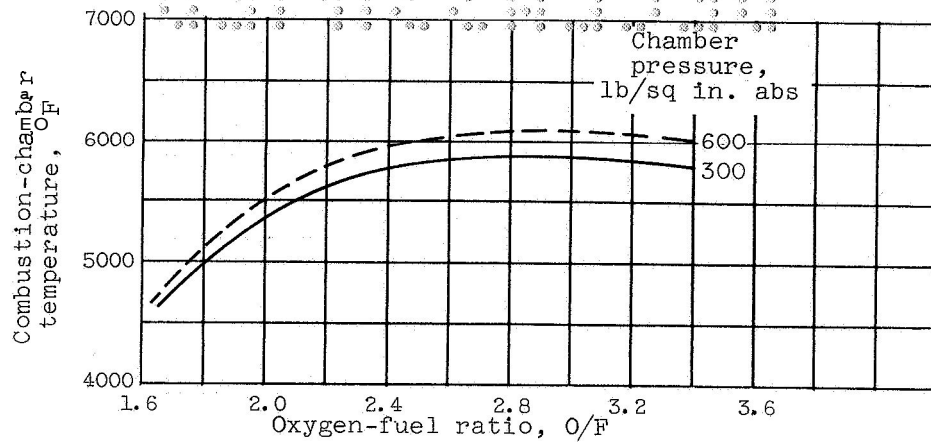
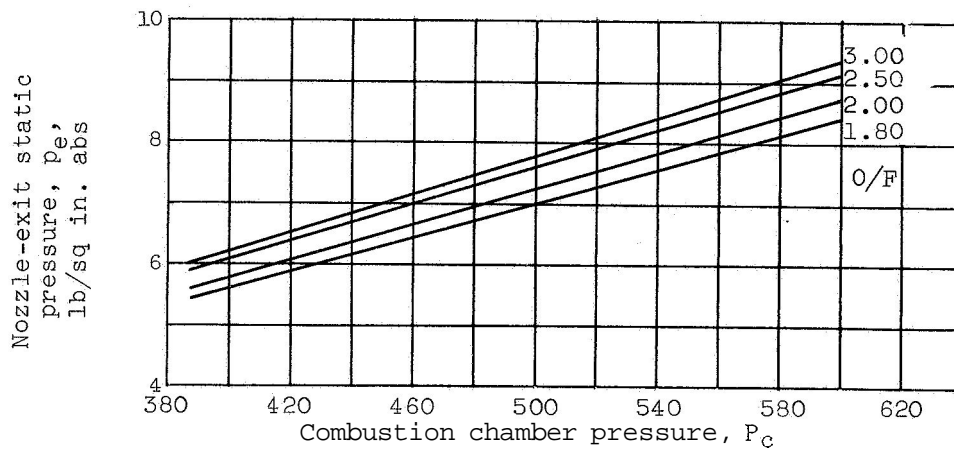


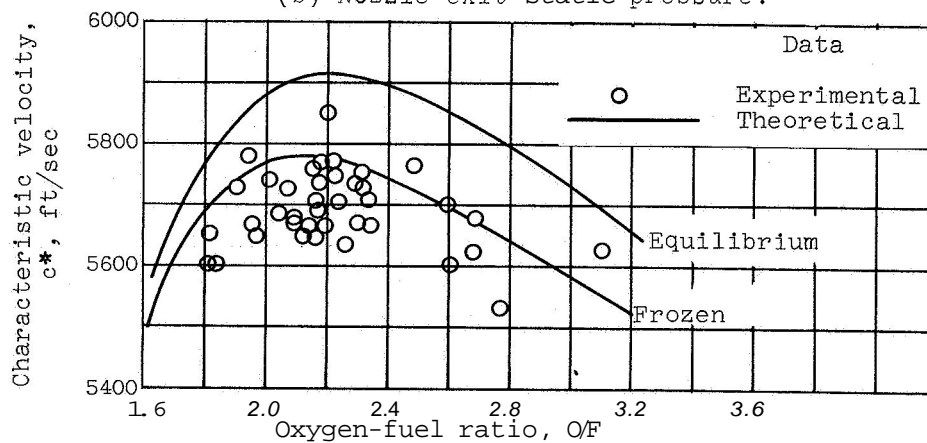
Figure 4. - Pitot-pressure boundary-layer profiles measured 16.29 inches upstream of the rocket exit.



(a) Combustion-chamber temperature.

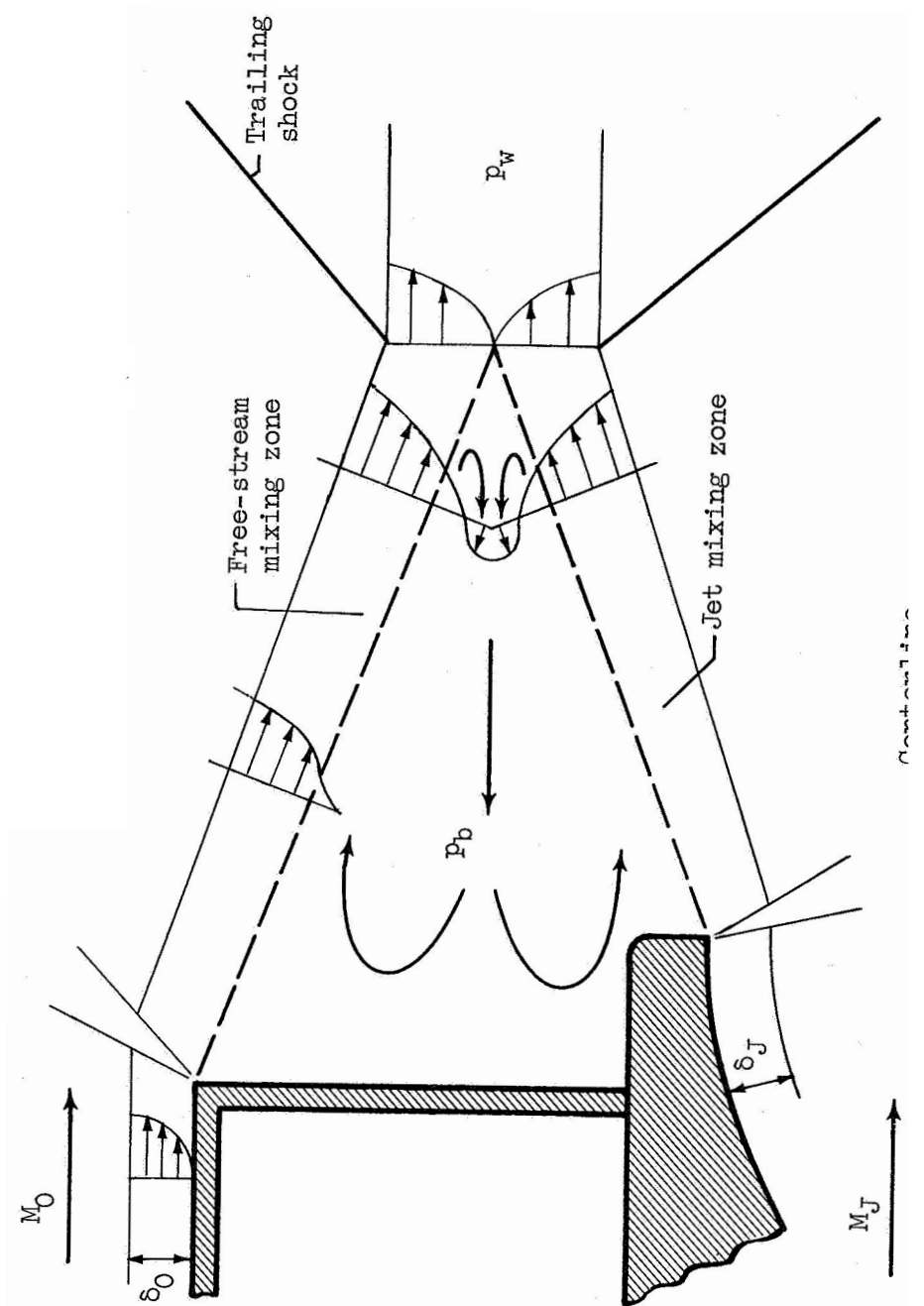


(b) Nozzle-exit static pressure.



(c) Characteristic velocity.

Figure 5. - Theoretical rocket performance for liquid oxygen and JP-4 with frozen composition during isentropic expansion (ref. 4).



CD-6662

Figure 6. - Theoretical flow in wake region.

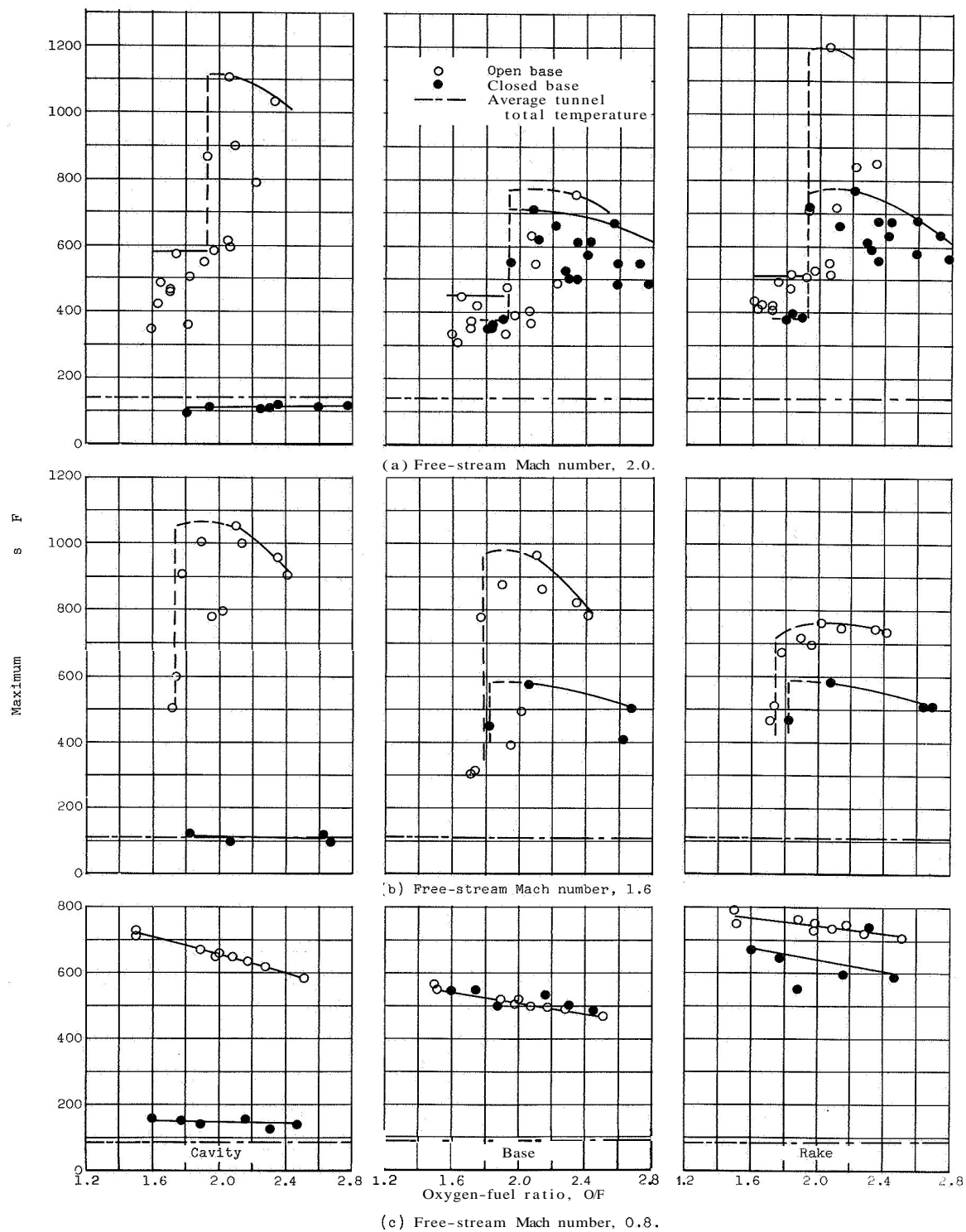
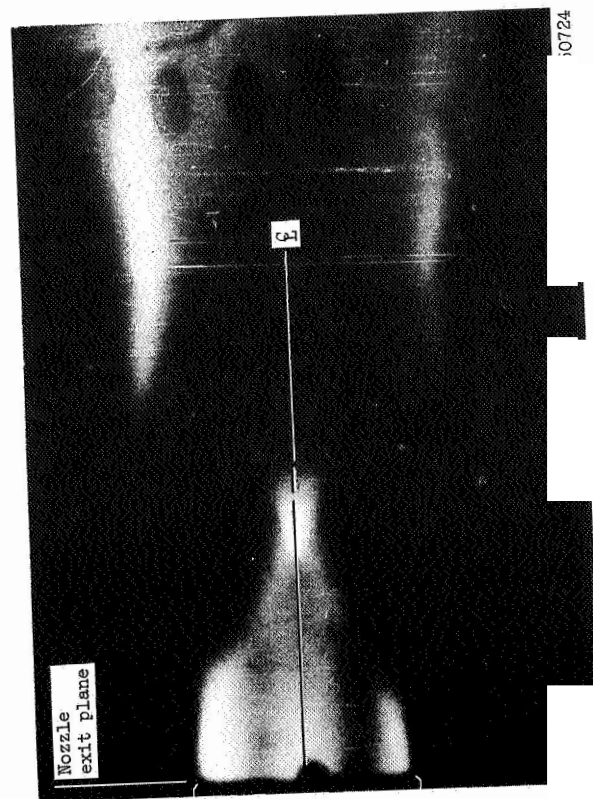
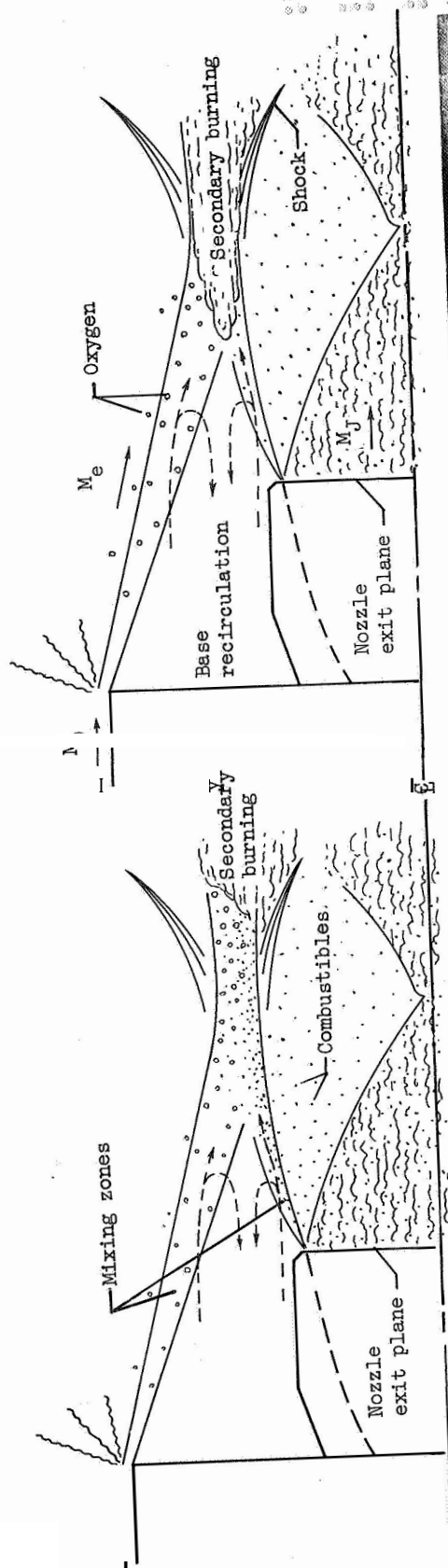
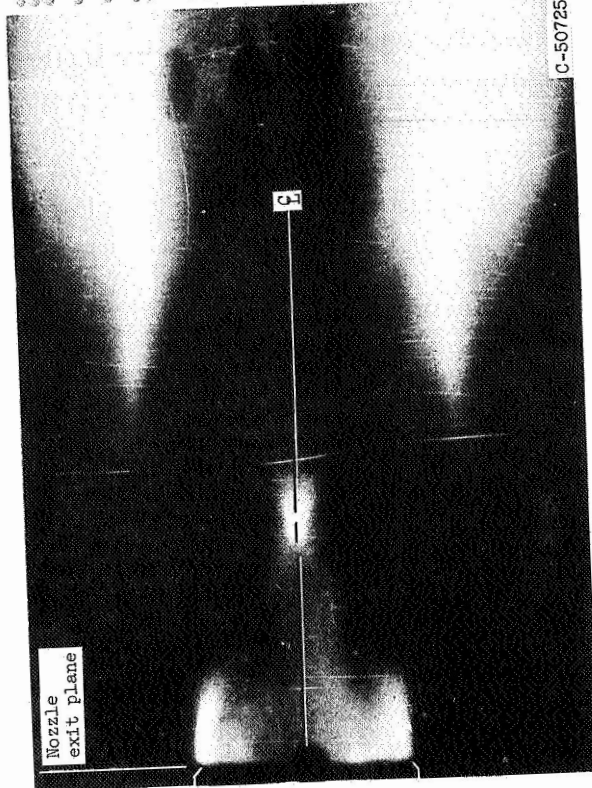


Figure 7. - Effect of oxygen-fuel ratio on temperatures with the 0.32 rocket extension ratio. Combustion chamber pressure, 500 pounds per square inch absolute.



(a) Oxidant-fuel ratio, 1.84; low base temperatures.



(b) Oxidant-fuel ratio, 2.31; high base temperatures.

Figure 8. - Schematic and photographic observations of the effect of oxidant-fuel ratio on base flow patterns. Chamber pressure, 500 pounds per square inch absolute.

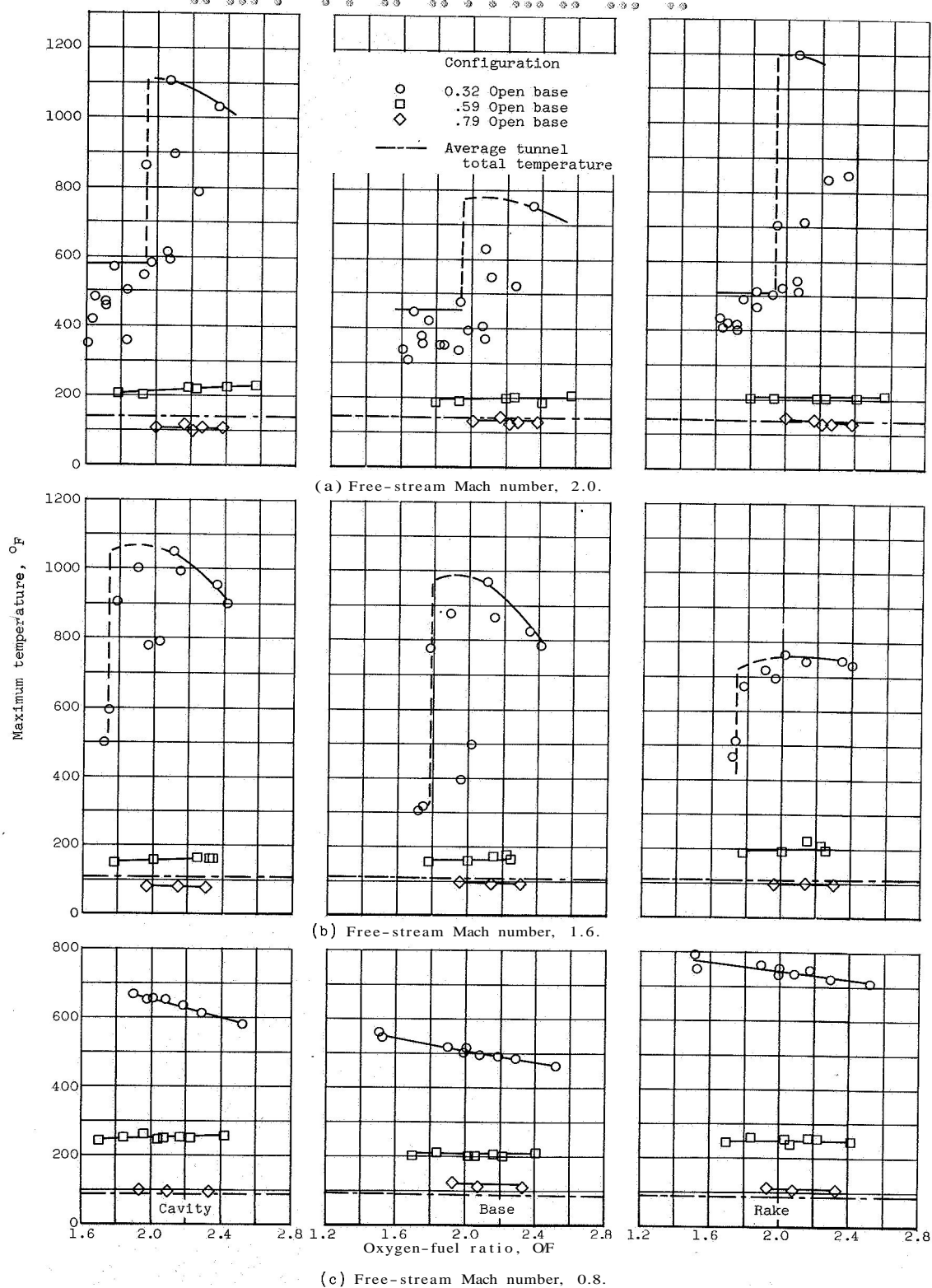


Figure 9. - Effect of rocket extension ratio on base region temperatures.
Combustion chamber pressure, 503 pounds per square inch absolute.

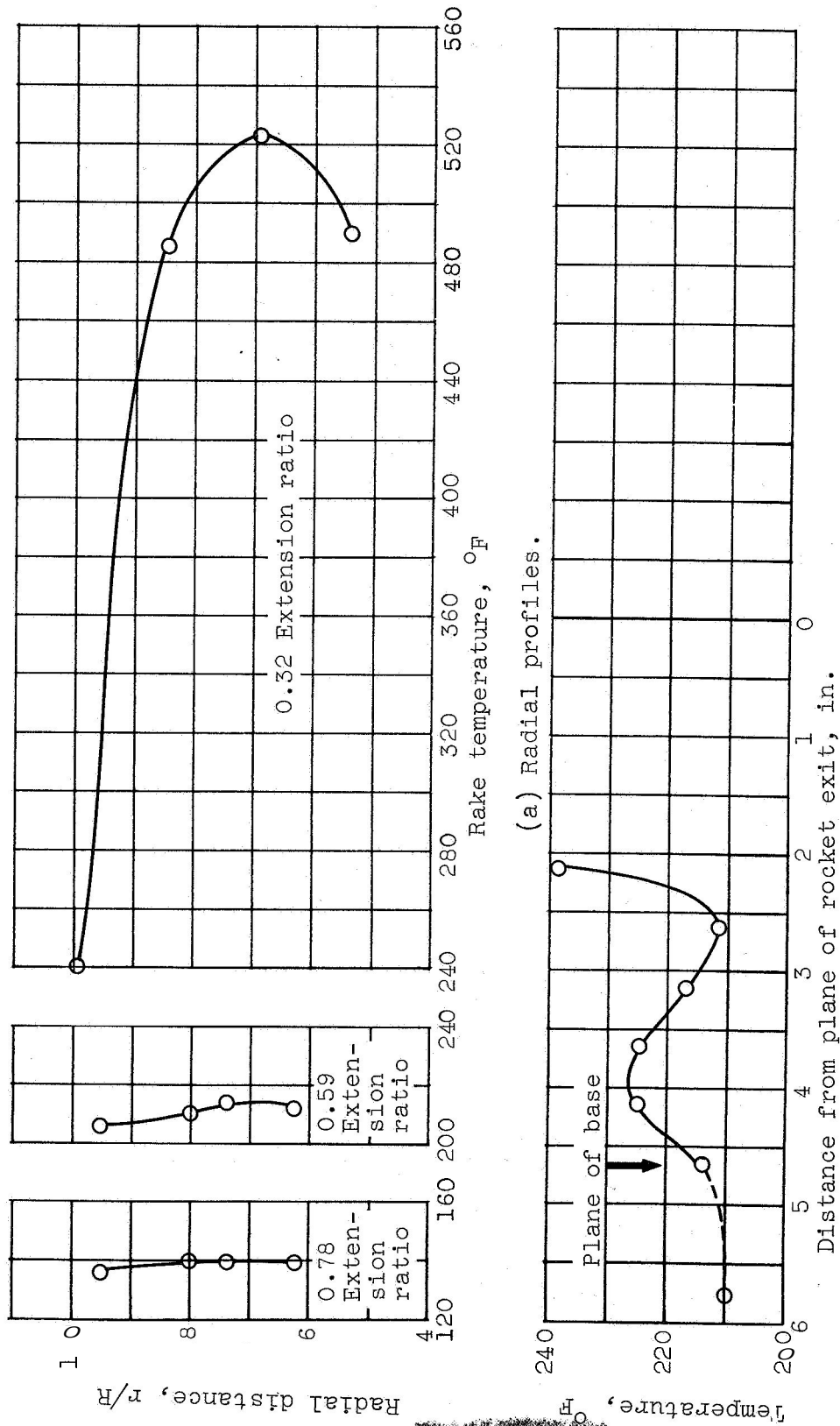
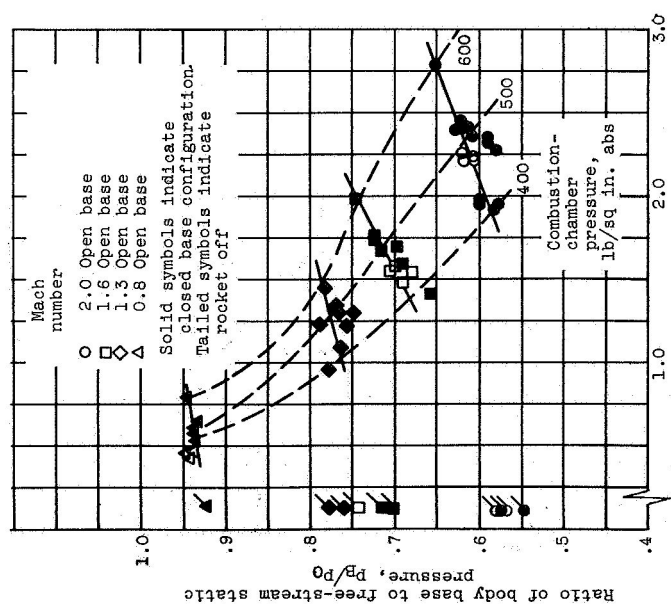
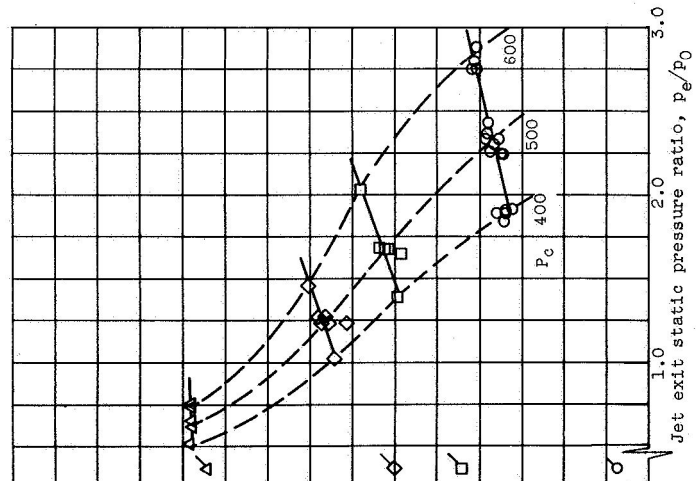


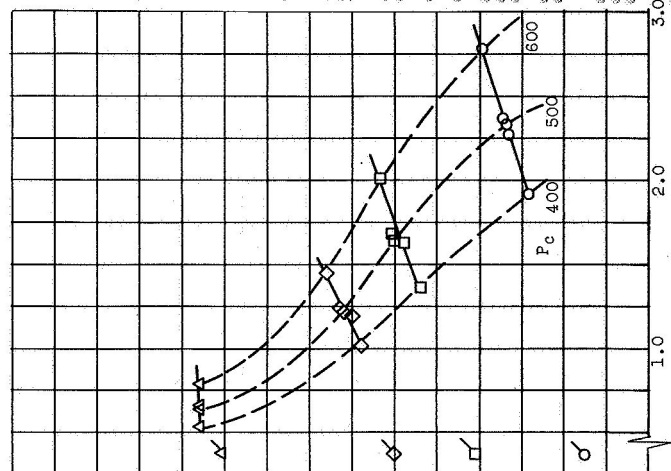
Figure 10. - Base region temperature profiles with open base. Combustion-chamber pressure, 500 pounds per square inch absolute; Mach number, 2.0; oxidant-fuel ratio, 2.2.



(a) Rocket extension ratio, 0.32.



(b) Rocket extension ratio, 0.59.



(c) Rocket extension ratio 0.74

Figure 11. - Effect of jet exit static pressure ratio on base pressure.

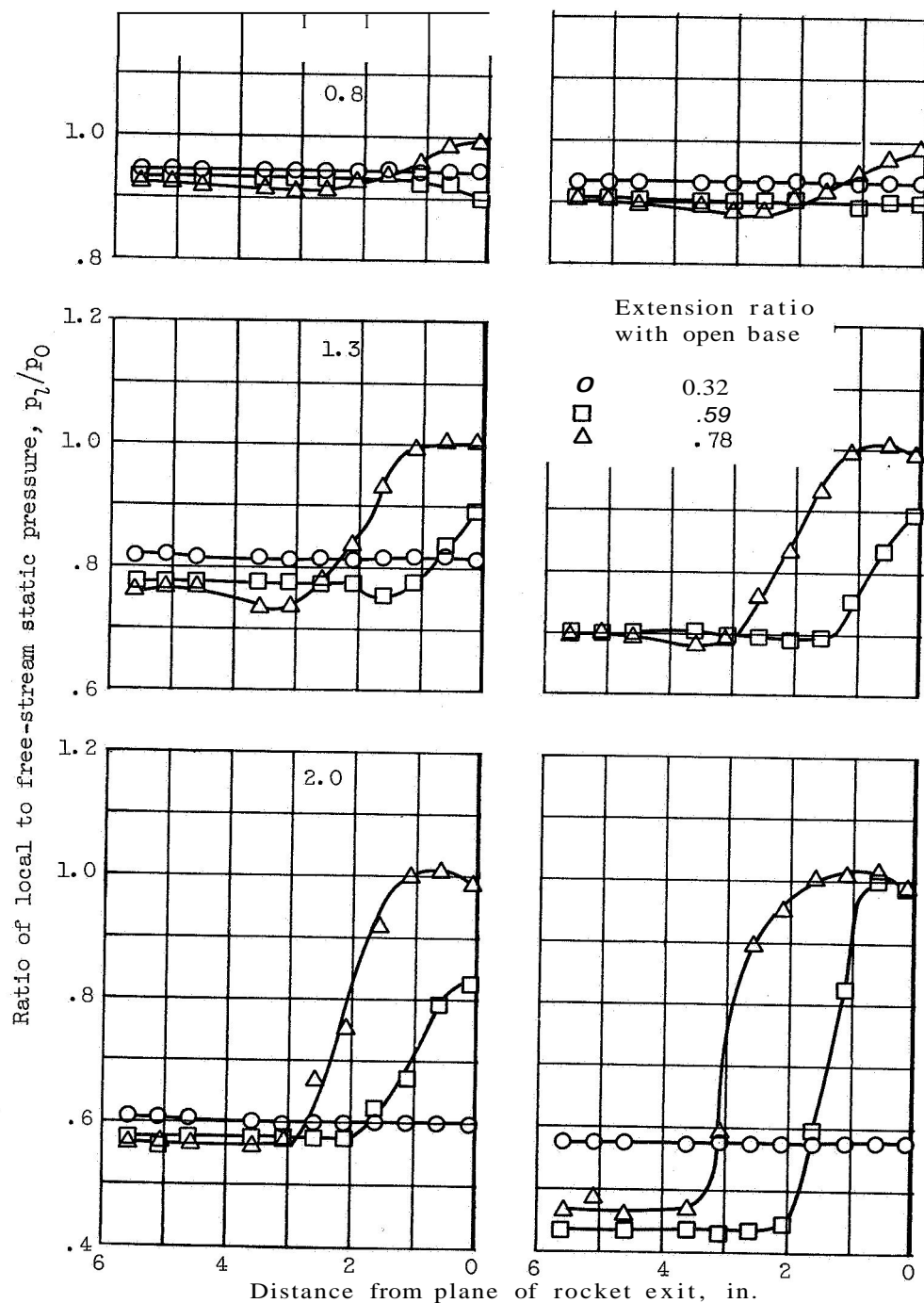
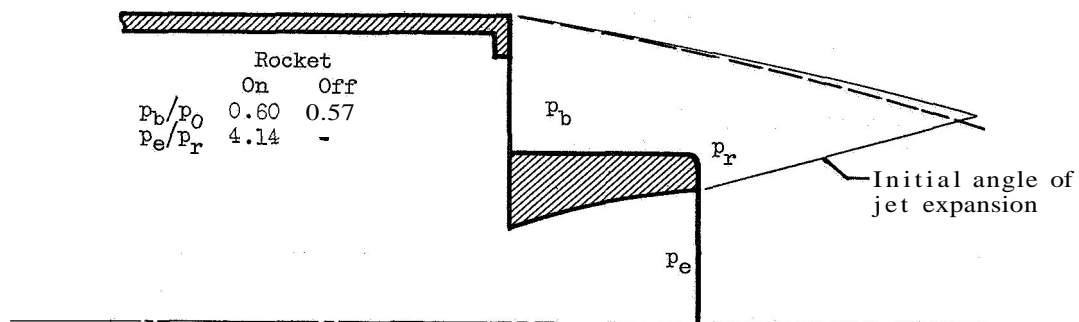
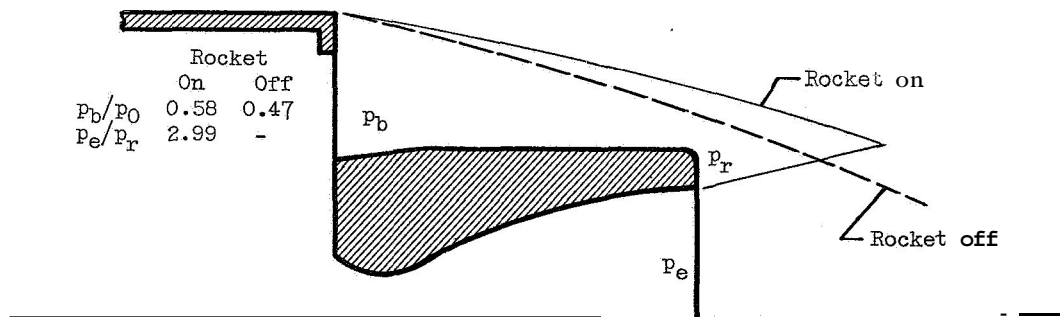


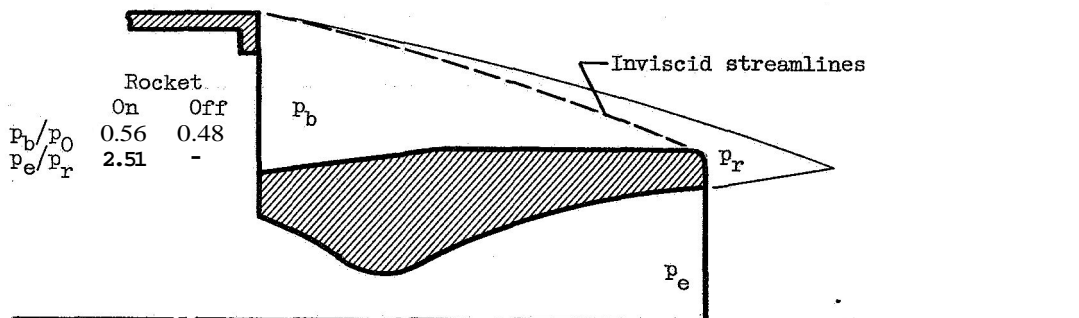
Figure 12. - Effect of rocket extension ratio on rocket motor external static-pressure distributions. Combustion-chamber pressure, 500 pounds per square inch absolute; oxygen-fuel ratio, 2.25.



(a) Rocket extension ratio, 0.32.



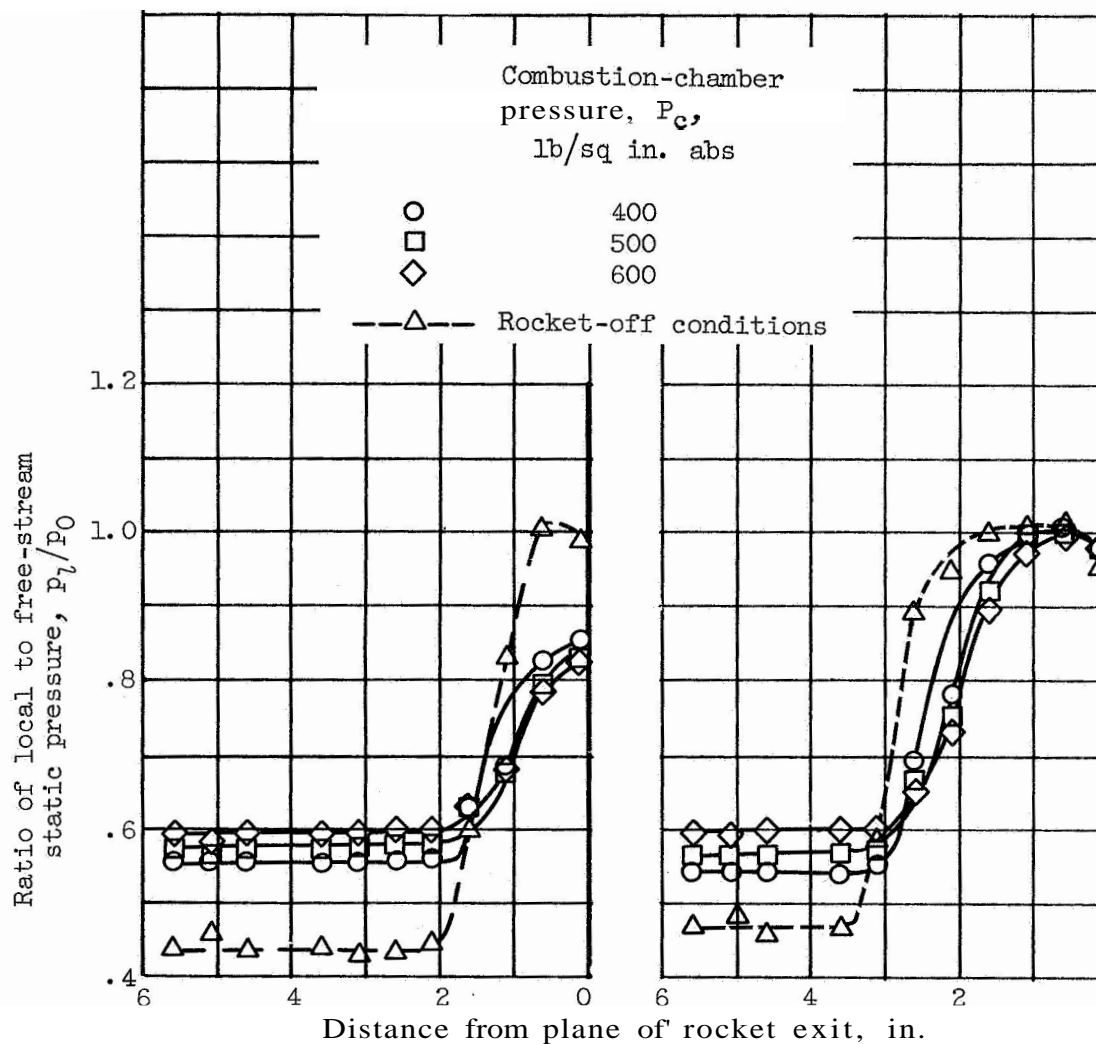
(b) Rocket extension ratio, 0.59.



(c) Rocket extension ratio, 0.78.

CD-6663

Figure 13. - Effect of rocket extension on analytical base region boundaries at Mach 2.0. Ratio of specific heats, 1.22.



(a) Rocket extension ratio, 0.59.

(b) Rocket extension ratio, 0.78.

Figure 14. - Effect of combustion-chamber pressure on rocket engine external pressure distributions. Mach number, 2.0; oxygen-fuel ratio, 2.25; open base configuration.

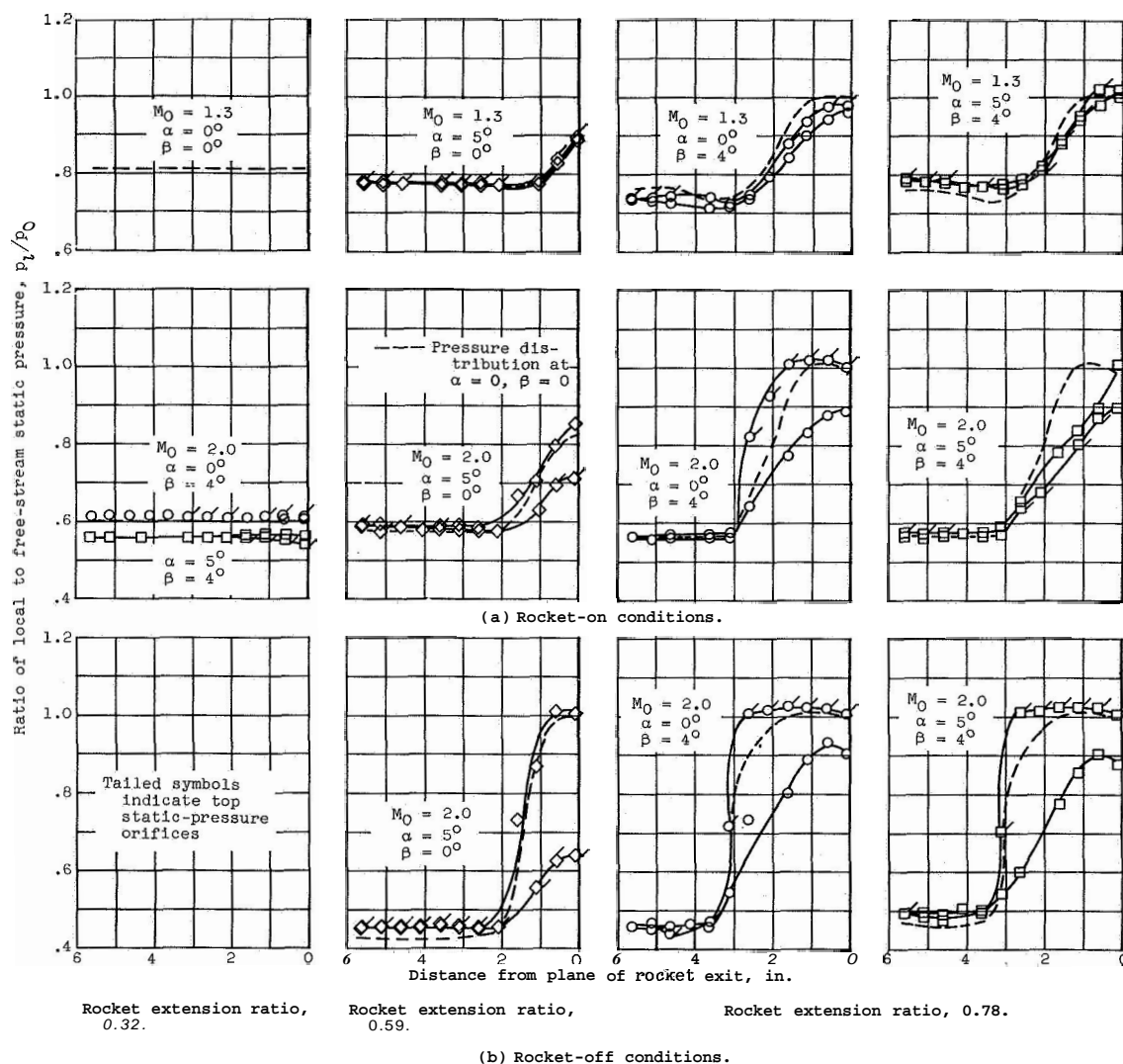
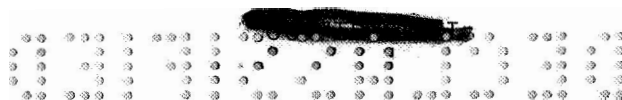
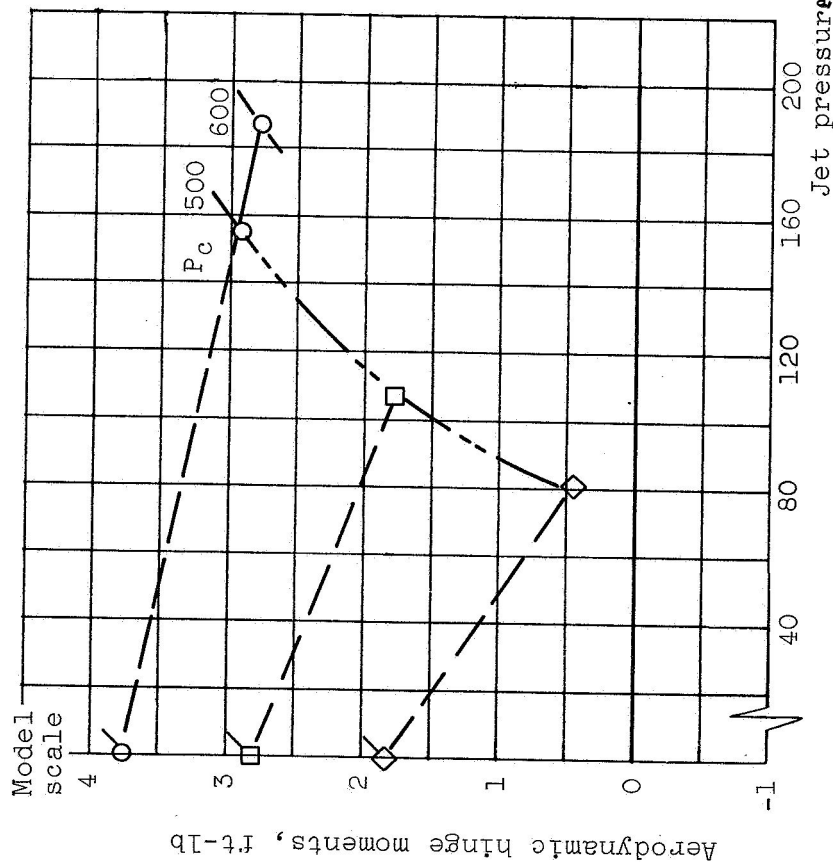
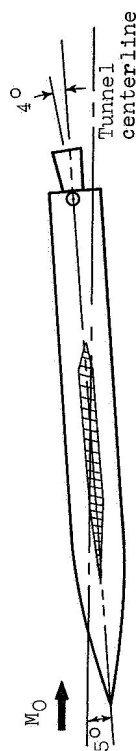
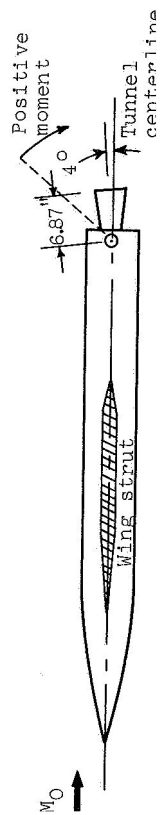
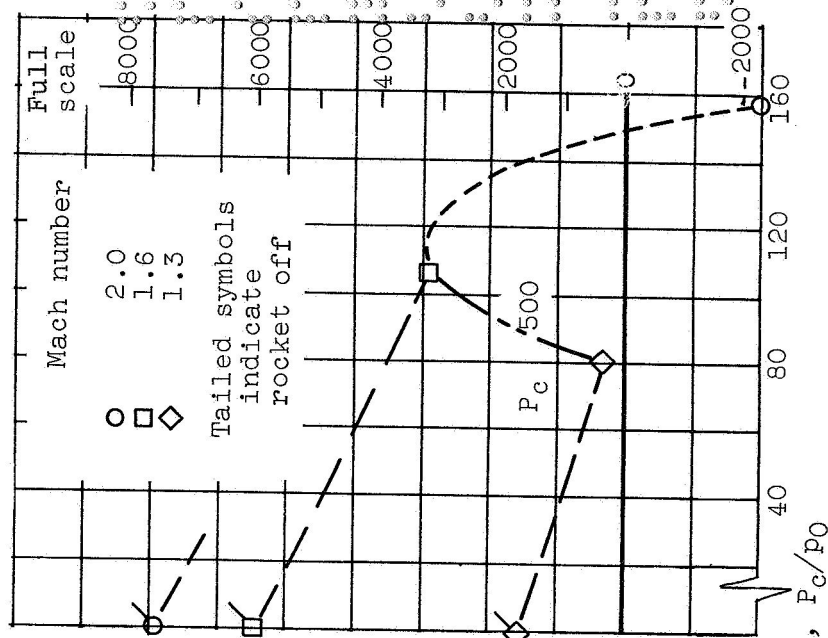


Figure 15. - Effect of gimbal angle and angle of attack on rocket engine external static-pressure distributions. Combustion-chamber pressure, 500 pounds per square inch absolute; oxidant-fuel ratio, 2.25; open base configuration.



(a) Angle of attack, 0° .



(b) Angle of attack, 5° .

Figure 16. - Aerodynamic hinge moments on a 4° gimbal rocket engine with a rocket extension ratio of 0.78.